Metallocene Catalysts for Olefin Polymerizations. XXIV. Stereoblock Propylene Polymerization Catalyzed by *rac*-[*anti*-Ethylidene(1-η^5-Tetramethylcyclopentadienyl)(1-η^5-Indenyl)dimethyltitanium: A Two-State Propagation*

JAMES C. W. CHIEN,[1a,†] GERALDO HIDALGO LLINAS,[1a] MARVIN D. RAUSCH,[1b] YE-GANG LIN,[1c] H. HENNING WINTER,[1c] JERRY L. ATWOOD,[2] and SIMON G. BOTT[2]

[1a]Department of Polymer Science and Engineering, [1b]Department of Chemistry, [1c]Department of Chemical Engineering, University of Massachusetts, Amherst, Massachusetts 01003, [2]Department of Chemistry, University of Alabama, Tuscaloosa, Alabama 35487

SYNOPSIS

Racemic-*anti*-[ethylidene(1-η^5-tetramethylcyclopentadienyl)(1-η^5-indenyl)dimethyltitanium (**6**) has been synthesized and its molecular structure determined by x-ray diffraction methods. The two Ti—Me(1) and Ti—Me(2) units have bond distances differing by 0.08 Å and their proton NMR resonances are separated by over 1 ppm. Using this compound and methylaluminoxane (MAO) as the activator, at 25°C the **6**/MAO catalyst produced polypropylene having crystalline domain with physical crosslinks. The polymers obtained at lower polymerization temperatures are rheologically liquids. The behaviors of this catalyst system resembles closely the previously reported *rac*-[*anti*-ethylidene(1-η^5-tetramethylcyclopentadienyl)(1-η^5-indenyl)dichlorotitanium (**4**)/MAO system. The structure of **6** determined here furnishes tangible support for the proposed two-state (isomeric)-switching propagation mechanism. Addition of MAO to **6** causes broadening of the Me(1) resonance in the ^{1}H-NMR spectra, and **6** is decomposed by $Ph_3C^+B(C_6F_5)_4^-$. © 1992 John Wiley & Sons, Inc.

Keywords: Ziegler–Natta catalysts • *ansa*-metallocene catalyst • thermoplastic elastomeric poly(propylene)

INTRODUCTION

Isotactic poly(propylene)s (*i*-PP) are manufactured with heterogeneous Ziegler–Natta catalysts. The earliest highly stereospecific catalyst was α-$TiCl_3$/$AlEt_2Cl$.[2] However, only a small fraction of the Ti in this catalyst was catalytically active. Since then, high activity $MgCl_2$ supported $TiCl_3$ catalysts[3] have been developed and are being used increasingly in the manufacturing of poly(propylene).

The new *ansa*-zirconocene catalysts, i.e., ethylene-bis(indenyl)dichlorozirconium (**1**, Et[Ind]$_2$-$ZrCl_2$) and ethylene-bis(tetrahydroindenyl)dichlorozirconium (**2**, Et[$IndH_4$]$_2ZrCl_2$) when activated with methylaluminoxane (MAO),[4,5] exhibit very high propylene polymerization activity. They have been said to produce 99+% *i*-PP[4a] and can be considered to be a well-defined single-site catalyst. In fact at temperatures of polymerization (T_p) of 50°C and above, no polymers were produced which have the set of physical and mechanical properties characteristic of commercial *i*-PP.[6] Radiolabeling of PP obtained with **2**/MAO[6c] revealed two catalytic states which gave PP's differing in MW and stereoregularity. In the case of the stereoelective polymerization of *rac*-4MH (4-methyl-1-hexene) by (S)-ethylene bis(1-indenyl)zirconium di-(0-acetyl-(R)-mandalate) (**3**),[7] there was a catalytic state which prefers reacting with the Re enantioface of

* See Reference 1.

† To whom all correspondence should be addressed.

Journal of Polymer Science: Part A: Polymer Chemistry, Vol. 30, 2601–2617 (1992)
 CCC 0887-624X/92/122601-17

Table I. Bond Distances and Angles for *rac*-[*anti*-Ethylidene(1-η^5-Tetramethylcyclopentadienyl)-(1-η^5-Indenyl)-dimethyltitanium (**6**)[a]

Atoms		Distance (Å)	Atoms		Distance (Å)
Ti	Me (1)	2.08 (1)	Ti	Me (2)	2.00 (1)
Ti	Ce (1)	2.07 (1)	Ti	Ce (2)	2.01 (1)
Ti	C (1)	2.21 (1)	Ti	C (2)	2.32 (1)
Ti	C (3)	2.44 (1)	Ti	C (4)	2.47 (1)
Ti	C (5)	2.37 (1)	Ti	C (7)	2.10 (1)
Ti	C (8)	2.17 (1)	Ti	C (9)	2.41 (1)
Ti	C (10)	2.56 (1)	Ti	C (15)	2.40 (1)
C (1)	C (2)	1.39 (1)	C (1)	C (5)	1.39 (1)
C (1)	C (6)	1.43 (1)	C (2)	C (3)	1.25 (1)
C (2)	C (21)	1.49 (1)	C (3)	C (4)	1.41 (1)
C (3)	C (31)	1.45 (2)	C (4)	C (5)	1.28 (1)
C (4)	C (41)	1.42 (1)	C (5)	C (51)	1.49 (2)
C (6)	C (7)	1.51 (1)	C (6)	C (61)	1.42 (1)
C (7)	C (8)	1.38 (1)	C (7)	C (15)	1.40 (1)
C (8)	C (9)	1.34 (1)	C (9)	C (10)	1.41 (2)
C (10)	C (11)	1.41 (2)	C (10)	C (15)	1.40 (1)
C (11)	C (12)	1.33 (2)	C (12)	C (13)	1.35 (2)
C (13)	C (14)	1.34 (1)	C (14)	C (15)	1.40 (1)

Atoms			Angle (deg)	Atoms			Angle (deg)
Me (1)	Ti	Me (2)	101.2 (5)	Me (1)	Ti	Ce (1)	107.9
Me (2)	Ti	Ce (1)	108.5	Me (1)	Ti	Ce (2)	106.5
Me (2)	Ti	Ce (2)	102.8	Ce (1)	Ti	Ce (2)	126.9
C (2)	C (1)	C (5)	113 (1)	C (2)	C (1)	C (6)	127 (1)
C (5)	C (1)	C (6)	116 (1)	C (1)	C (2)	C (3)	105 (1)
C (1)	C (2)	C (21)	133 (1)	C (3)	C (2)	C (21)	122 (1)
C (2)	C (3)	C (4)	108 (1)	C (2)	C (3)	C (31)	123 (1)
C (4)	C (3)	C (31)	129 (1)	C (3)	C (4)	C (5)	114 (1)
C (3)	C (4)	C (41)	125 (1)	C (5)	C (4)	C (41)	121 (1)
C (1)	C (5)	C (4)	100 (1)	C (1)	C (5)	C (51)	132 (1)
C (4)	C (5)	C (51)	128 (1)	C (1)	C (6)	C (7)	105.4 (9)
C (1)	C (6)	C (61)	112 (1)	C (7)	C (6)	C (61)	114 (1)
C (6)	C (7)	C (8)	123 (1)	C (6)	C (7)	C (15)	123 (1)
C (8)	C (7)	C (15)	111 (1)	C (7)	C (8)	C (9)	108 (1)
C (8)	C (9)	C (10)	108 (1)	C (9)	C (10)	C (11)	101 (1)
C (9)	C (10)	C (15)	109 (1)	C (11)	C (10)	C (15)	116 (1)
C (10)	C (11)	C (12)	120 (1)	C (11)	C (12)	C (13)	123 (1)
C (12)	C (13)	C (14)	120 (1)	C (13)	C (14)	C (15)	119 (1)
C (7)	C (15)	C (10)	103 (1)	C (7)	C (15)	C (14)	135 (1)
C (10)	C (15)	C (14)	122 (1)				

Atoms			Angle (deg)	Atoms			Angle (deg)
Me (1)	-Ti	-C (1)	124.0 (5)	Me (2)	-Ti	-C (1)	121.7 (5)
Me (1)	-Ti	-C (2)	88.7 (5)	Me (2)	-Ti	-C (2)	136.8 (4)
C (1)	-Ti	-C (2)	35.5 (4)	Me (1)	-Ti	-C (3)	80.8 (5)
Me (2)	-Ti	-C (3)	109.6 (4)	C (1)	-Ti	-C (3)	53.3 (4)
C (2)	-Ti	-C (3)	30.2 (3)	Me (1)	-Ti	-C (4)	106.5 (5)

Table I. *Continued*

Atoms			Angle (deg)	Atoms			Angle (deg)
Me (2)	-Ti	-C (4)	83.8 (4)	C (1)	-Ti	-C (4)	51.6 (4)
C (2)	-Ti	-C (4)	53.3 (4)	C (3)	-Ti	-C (4)	33.4 (3)
Me (1)	-Ti	-C (5)	135.7 (5)	Me (2)	-Ti	-C (5)	87.2 (5)
C (1)	-Ti	-C (5)	35.0 (3)	C (2)	-Ti	-C (5)	58.8 (4)
C (3)	-Ti	-C (5)	55.8 (4)	C (4)	-Ti	-C (5)	30.6 (3)
Me (1)	-Ti	-C (7)	125.3 (5)	Me (2)	-Ti	-C (7)	117.8 (5)
C (1)	-Ti	-C (7)	65.7 (4)	C (2)	-Ti	-C (7)	87.5 (4)
C (3)	-Ti	-C (7)	115.9 (4)	C (4)	-Ti	-C (7)	114.0 (4)
C (5)	-Ti	-C (7)	85.5 (4)	Me (1)	-Ti	-C (8)	87.8 (5)
Me (2)	-Ti	-C (8)	133.5 (5)	C (1)	-Ti	-C (8)	86.9 (4)
C (2)	-Ti	-C (8)	88.3 (4)	C (3)	-Ti	-C (8)	116.8 (4)
C (4)	-Ti	-C (8)	137.5 (4)	C (5)	-Ti	-C (8)	117.5 (4)
C (7)	-Ti	-C (8)	37.6 (4)	Me (1)	-Ti	-C (9)	77.9 (5)
Me (2)	-Ti	-C (9)	103.7 (5)	C (1)	-Ti	-C (9)	119.1 (4)
C (2)	-Ti	-C (9)	119.5 (4)	C (3)	-Ti	-C (9)	143.2 (4)
C (4)	-Ti	-C (9)	170.7 (4)	C (5)	-Ti	-C (9)	142.6 (4)
C (7)	-Ti	-C (9)	57.6 (5)	C (8)	-Ti	-C (9)	33.4 (4)
Me (1)	-Ti	-C (10)	102.7 (5)	Me (2)	-Ti	-C (10)	78.2 (4)
C (1)	-Ti	-C (10)	118.9 (4)	C (2)	-Ti	-C (10)	140.8 (4)
C (3)	-Ti	-C (10)	170.8 (4)	C (4)	-Ti	-C (10)	148.1 (4)
C (5)	-Ti	-C (10)	121.5 (4)	C (7)	-Ti	-C (10)	55.1 (4)
C (8)	-Ti	-C (10)	55.4 (4)	C (9)	-Ti	-C (10)	32.8 (4)
Me (1)	-Ti	-C (15)	133.9 (5)	Me (2)	-Ti	-C (15)	83.1 (4)
C (1)	-Ti	-C (15)	88.7 (4)	C (2)	-Ti	-C (15)	119.4 (4)
C (3)	-Ti	-C (15)	141.4 (4)	C (4)	-Ti	-C (15)	119.6 (4)
C (5)	-Ti	-C (15)	90.1 (4)	C (7)	-Ti	-C (15)	35.4 (4)
C (8)	-Ti	-C (15)	59.9 (4)	C (9)	-Ti	-C (15)	56.9 (4)
C (10)	-Ti	-C (15)	32.5 (3)	Ti	-C (1)	-C (2)	76.9 (7)
Ti	-C (1)	-C (5)	79.0 (6)	Ti	-C (1)	-C (6)	93.4 (7)
Ti	-C (2)	-C (1)	67.6 (6)	Ti	-C (2)	-C (3)	80.2 (8)
Ti	-C (2)	-C (21)	123.4 (7)	Ti	-C (3)	-C (2)	69.6 (8)
Ti	-C (3)	-C (4)	74.1 (7)	Ti	-C (3)	-C (31)	129.5 (9)
Ti	-C (4)	-C (3)	72.4 (7)	Ti	-C (4)	-C (5)	70.7 (7)
Ti	-C (4)	-C (41)	127.0 (9)	Ti	-C (5)	-C (1)	66.0 (6)
Ti	-C (5)	-C (4)	78.7 (7)	Ti	-C (5)	-C (51)	123.3 (8)
Ti	-C (7)	-C (6)	95.2 (7)	Ti	-C (7)	-C (8)	73.9 (7)
Ti	-C (7)	-C (15)	84.1 (6)	Ti	-C (8)	-C (7)	68.5 (6)
Ti	-C (8)	-C (9)	83.1 (8)	Ti	-C (9)	-C (8)	63.5 (7)
Ti	-C (9)	-C (10)	79.5 (7)	Ti	-C (10)	-C (9)	67.8 (7)
Ti	-C (10)	-C (11)	131.1 (8)	Ti	-C (10)	-C (15)	67.6 (7)
Ti	-C (15)	-C (7)	60.5 (6)	Ti	-C (15)	-C (10)	79.9 (7)
Ti	-C (15)	-C (14)	126.4 (8)				

[a] Ce (1) is centroid of C1–C5; Ce (2) is centroid of C7–C10 and C15.

the monomer, and another state which prefers insertions involving the Si face of 4MH.

Observations are accumulating which suggest the existence of two (or more) propagating states that can interconvert during the growth of a macromolecular chain. To test this possibility, a nonsymmetric compound *rac*-[*anti*-ethylidene(1-η^5-tetramethylcyclopentadienyl)(1-η^5-indenyl) dichlorotitanium (**4**) (and also the *syn* diastereomer **5**) was synthesized and used to polymerize propylene.[8] The PP obtained at T_p = 25 and 50°C were found to have the characteristic properties of a thermoplastic elastomer (TPE).[8,9] The macromolecular chain is comprised of n alternating blocks of a number of

amorphous/stereoirregular propylene units, (*am*-PP)$_a$, and *c* number of crystallizable/stereoregular propylene units, (*cry*-PP)$_c$. It was possible to obtain a estimates for such multiblock molecular structure using equilibrium modulus, GPC, and x-ray diffraction. The structures are approximately [(*am*-PP)$_{50}$(*cry*-PP)$_{18}$]$_{34}$ and [(*am*-PP)$_{105}$(*cry*-PP)$_{46}$]$_{10}$ for the TPE–PP obtained by 25 and 50°C polymerizations, respectively. The production of alternate crystallizable and amorphous segment in a single macromolecular chain can be readily explained by the existence of two interconverting states which catalyze propylene insertions with different stereoselectivities.

Unfavorable crystallization behavior of **4** prevented its x-ray structure determination. We have now synthesized the title compound **6**, grown single crystals, and determined its x-ray structure.[10] Furthermore, **6** and its *syn* diastereomer (**7**) have nonequivalent Ti–methyl bonds according to NMR. The kinetics of propylene polymerization by **6**/MAO had been determined and compared with those of the **4**/MAO systems. These results lend support to the two-state switching propagation mechanism.

EXPERIMENTAL

Synthesis

All chemicals and solvents were purchased from Aldrich. Solvents were purified by standard methods.[11]

Compound **4** was synthesized in 95% yield by the reaction of ethylidene(1-η^5-tetramethylcyclopentadienyl)(1-η^5-indenyl)dilithium (**8**) suspended in 2/1 *n*-hexane/diethyl ether with $TiCl_4 \cdot 2THF$ between −25 and +25°C as previously described.[8b] Subsequently we found that the same reaction of **8** with $TiCl_4$ in diethyl ether afforded an equimolar mixture of the diastereomers **4** and **5**.

Compound **6** was synthesized as follows. To a suspension of **4** (0.5 g, 1.3 mmol) in 15 mL of *n*-hexane was added dropwise 1.6 mL of methyllithium (1.6*M*, 2.6 mmol) at room temperature and the mixture stirred for 6 h. After titration, concentrating, and cooling at −20°C, orange red crystals of **6** were obtained in 60% yield.

ANAL. Calcd: C, 77.2% (77.66%); H, 8.18% (8.23%).

Crystals suitable for the x-ray diffraction study were grown by the slow cooling of a hexane solution of **6** at −20°C. Similar reaction conditions were used to convert the diastereomeric mixture of **4** and **5** to the corresponding dimethyl compounds **6** and **7**.

MAO was synthesized as previously described.[12] Triphenylcarbenium (trityl) tetrakis(pentafluorophenyl)borate (**9**) was prepared by mixing LiB$(C_6F_5)_4$[13] with 20% excess triphenylmethyl chloride in 200 mL of dry *n*-hexane and refluxing overnight.[14] Recrystallization of the crude product afforded orange crystals of **9** in 64% yield which exhibited the correct elemental analysis and expected NMR spectra.[14]

Polymerization and Kinetics

Polymerizations were carried out in a 250 mL crown-capped glass pressure reactor with magnetic stirring.[15] Purified toluene (50–100 mL) and MAO were introduced under argon and the reactor capped. The reactor was immersed in a constant temperature bath, evacuated, then saturated with propylene. The solubility of propylene at 1.7 atm in toluene was determined as a function of temperature; it is 0.47, 0.73, and 0.94*M* at 25, 0 and −20°C, respectively. Polymerization began immediately following injection of the catalyst (20 mg of **6** in 10 mL toluene).

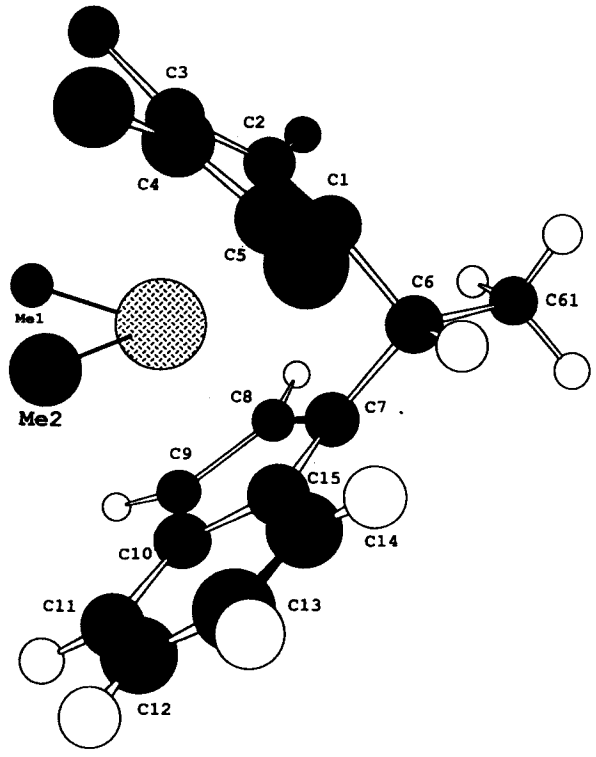

Figure 1. Molecular structure of *rac*-[*anti*-ethylidene(1-η^5-tetramethylcyclopentadienyl)(1-η^5-indenyl)-dimethyltitanium (**6**).

Polymerization was quenched with methanol at the desired time (t_p), and the polymer worked up by a standard procedure.[15] From the data of polymer yield (Y) versus t_p, we calculated the rate of polymerization (R_p) as a function of t_p.

The metal polymer bond concentration ([MPB] = [Ti—P] + [Al—P]) was determined by quenching the polymerization mixture with CH_3O^3H (24.1 mCi/mol) and radioassay.[16] The kinetic isotope effect for the **6**/MAO system was taken to be 1.53, the same as that found for the **4**/MAO system.[8]

Polymer Characterization

Intrinsic viscosity ([η]) of PP was measured in decalin at 135°C using an Ubbelohde viscometer.

Dynamic mechanical measurement was made on a Rheometrics Dynamic Spectrometer (RDS Model 7700) using a cone/plate geometry. Samples were molded in the rheometer usually at 75°C but also at higher temperatures for some specimens. Samples for mechanical elastic property measurements were molded at 120°C into a dogbone shape; the dimension for the extension part was $20 \times 5 \times 0.5$ mm^3. After cooling to ambient temperature, the specimens were stored for three days prior to the mechanical tests. The specimens were extended at 20 cm/min, using an Instron Model TTBN tensile machine.

RESULTS

X-Ray Diffraction

The space group of **6** is found to be $P2_1/c$, and the unit cell parameters are a = 11.220(1) Å, b = 9.366(2) Å, c = 18.470(3) Å; β = 106.75(1)°; and D_c = 1.22 g cm^{-3} for Z = 4. Least-squares refinement based on 729 observed reflections produced the final discrepancy indicies R = 0.054 and R_w = 0.056. Table I gives the bond distances and angles.

Figure 1 shows the x-ray molecular structure of **6**. The methyl group attached to the bridging carbon atom C_6 is oriented in an anti arrangement relative to the six-membered ring of the indenyl ligand, consistent with the geometry proposed previously for **4** on the basis of steric considerations.[8] The two σ-bonded methyl substitutents are located in sterically nonequivalent positions, with Me(2) oriented toward the six-membered ring of the indenyl ligand. Furthermore, the Ti—CH_3 distances are significantly different, with Ti—Me(1) = 2.08(1) Å and Ti—Me(2) = 2.00(1) Å. Both of these Ti—CH_3 separations are distinctly shorter than the Ti—CH_3 distance of 2.21(2) Å found in (η^5-$C_9H_7)_2Ti(CH_3)_2$.[17] The C—C distances in the ethylidene bridge are also different, being 1.43 Å (C1–C6) toward the Cp* ring as compared to 1.51 Å (C6–C7) toward the indenyl ring for a difference of 0.08

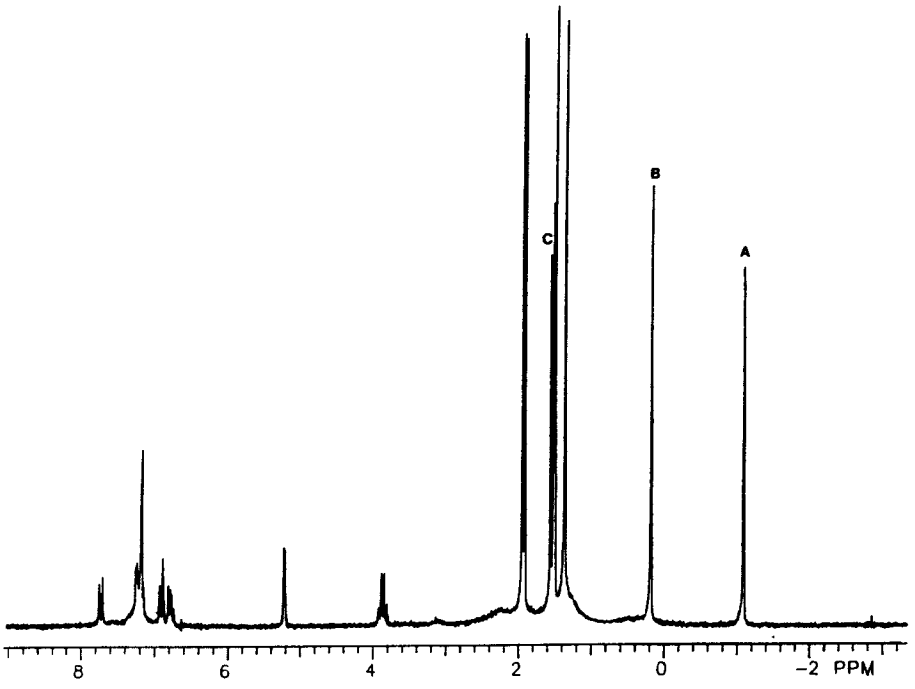

Figure 2. ^{1}H-NMR spectra of **6** in C_6D_6.

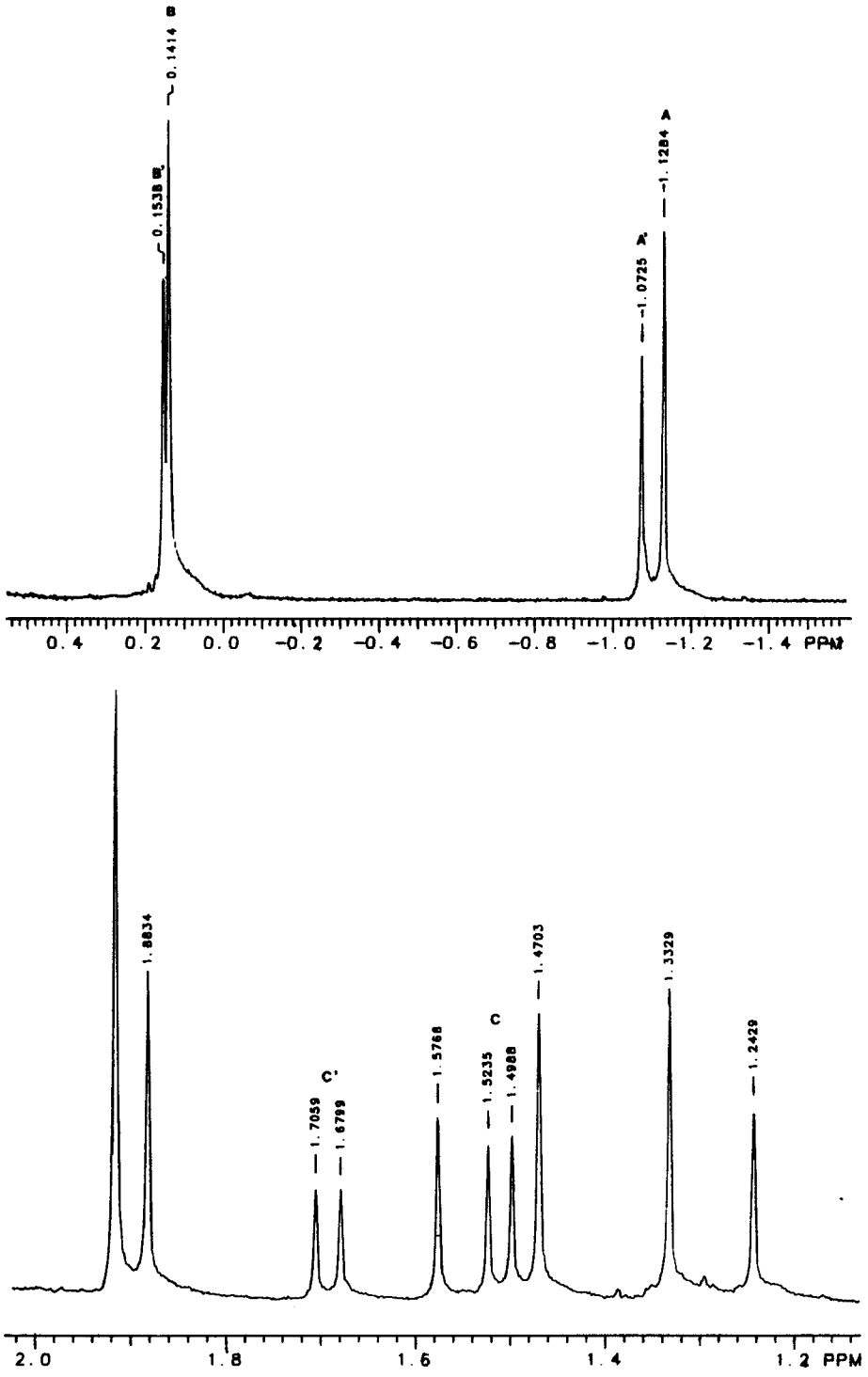

Figure 3. ^{1}H-NMR spectra of **6/7** mixture in C_6D_6.

Å. The degree of canting between the two hapto-bonded rings is indicated by the angle ϕ ascribed by the ring (Ind) centroid-Ti-ring (Cp*) centroid. An increase of either the number or size of bridged atoms results in a lowering of the degree of canting (increase of ϕ) as the two rings become more parallel to one another.[18] The value of ϕ is 127.0° for **6**. The angle ϕ increases to 128.2°, 128.7°, and 133° as the number and size of bridging atoms increases in $[C_2H_4(C_5H_4)_2]TiCl_2$,[19] $[Si(CH_3)_2(C_5H_4)_2]TiCl_2$,[18]

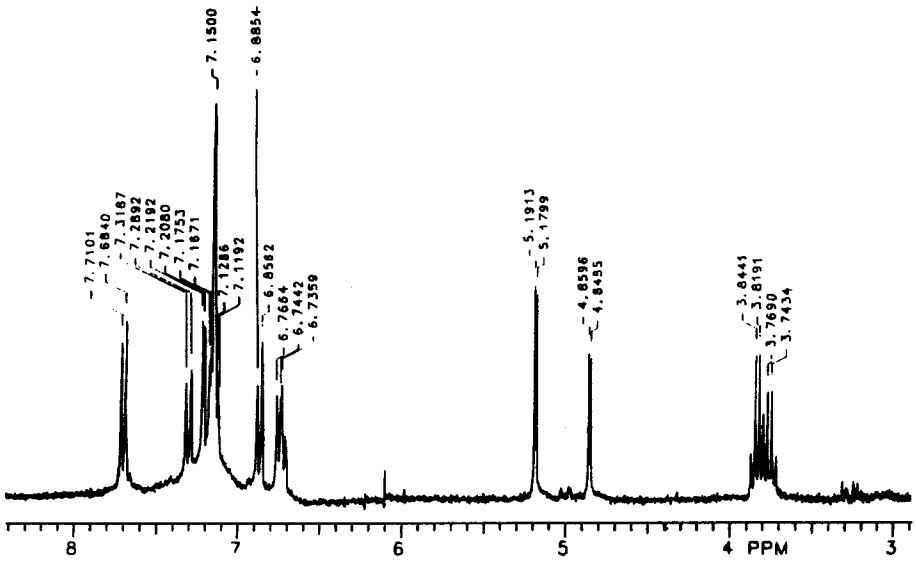

Figure 3 *(continued from the previous page)*

and $[C_3H_6(C_5H_4)_2]_2TiCl_2$,[21], respectively. Conversely, $[CH_2(C_5H_4)_2]TiCl_2$[18] has a smaller ϕ of 121°.

The Ti atom is significantly closer to the indenyl ring than the Cp* ring. This result and the longer C6–indenyl distance than C6–Cp* distance (*vide supra*) may be due to a difference in the hapticity of the two ring systems. In this regard, the bond distances for C7–C8(1.38 Å) and C8–C9(1.34 Å) are noticeably shorter than C9–C10(1.41 Å), C10–C15(1.40 Å), and C7–C15(1.40 Å).

NMR

The ^{1}H-NMR spectra of **6** and the **6/7** diastereomeric mixture are given in Figures 2 and 3, respectively. The singlets designated as A and B and the doublet designated as C can be assigned to the Ti—Me(1), Ti—Me(2) and C_6—Me (ethylidene methyl) resonances, respectively. The chemical shifts assignments are summarized in Table II.

Propylene was polymerized in NMR sample tubes. In these experiments, a toluene solution of **6**

Table II. ^{1}H-NMR Parameters[a] for nCompounds **6** and **7**

anti-Diastereomer (**6**)			*syn*-Diastereomer (**7**)		
δ (ppm)	m, J (Hz)	Protons	δ (ppm)	m, J (Hz)	Protons
7.69	d, 5.2	1H	7.29	d, 5.9	1H
7.20	m	2H	7.20	m	2H
6.87	d, 5.8	1H	6.87	d, 5.8	1H
6.74	m	1H	6.74	m	1H
5.18	d, 2.3	1H	4.85	d, 2.2	1H
3.83	q, 5.0	1H	3.75	q, 5.1	1H
1.92	s	3H	1.92	s	6H
1.88	s	3H	1.69	d, 5.2	3H
1.50	d, 4.9	3H	1.57	s	3H
1.47	s	3H	1.24	s	3H
1.33	s	3H	0.15	s	3H
0.14	s	3H	−1.07	s	3H
−1.12	s	3H			

[a] Solvent is C_6D_6.

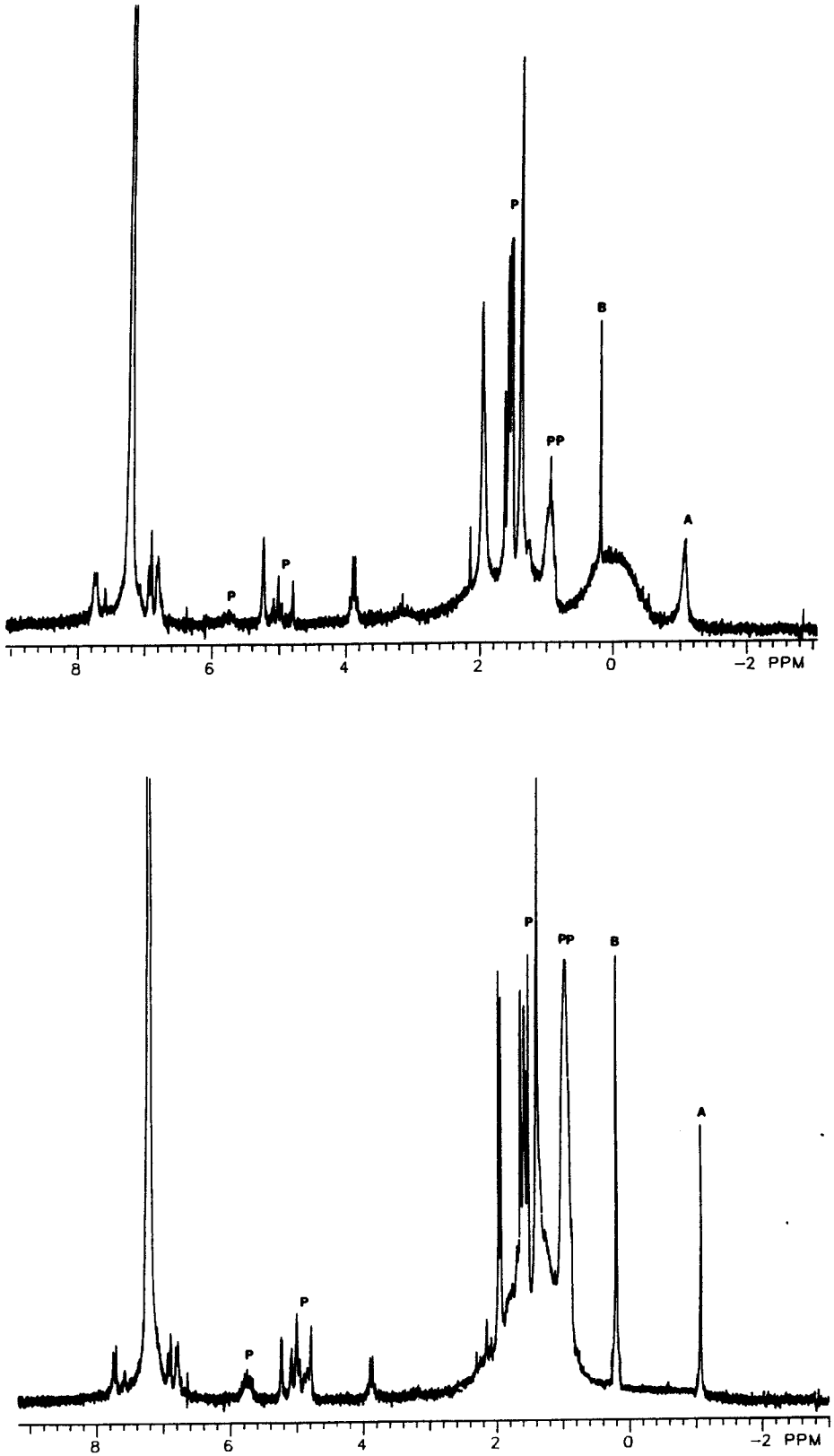

Figure 4. ^{1}H-NMR of a propylene polymerization mixture catalyzed by **6**/MAO: (a) immediately upon mixing, (b) 45 min after mixing.

was saturated with propylene, MAO was introduced and the ^{1}H-NMR spectrum was continuously monitored. Immediately after the addition of MAO, the Ti—Me(1) peak suffered significant line broadening; the resonance decreased in peak height but gained in width [Fig. 4(a)]. There was observed a new broad peak (ca. 0.8 ppm FWHH) at about 0 ppm due to the MAO. Resonances of propylene and PP were also clearly present. No signal indicative of a Ti^+ — Me species was detected. The following spectral changes were observed for a reaction time of about 15 min. The peak intensity of Ti—Me(2) decreased while that of Ti—Me(1) increased. The broad MAO resonance at 0 ppm decreased in size with a concomittent increase of the broad base beneath the aliphatic protons (1–2 ppm). This change continued with time; the Ti—Me(1) line began to narrow 30 min after mixing. The spectra at 45 min is shown in Figure 4(b); it contained very narrow signals for Ti—Me(1) and Ti—Me(2) with the latter being noticeably more intense. The MAO resonances either lie entirely beneath the aliphatic proton region or are too broad to be observed. The PP resonances are very prominent.

An NMR study was also made on the reaction between **6/7** with **9**, which represents a way to pro-

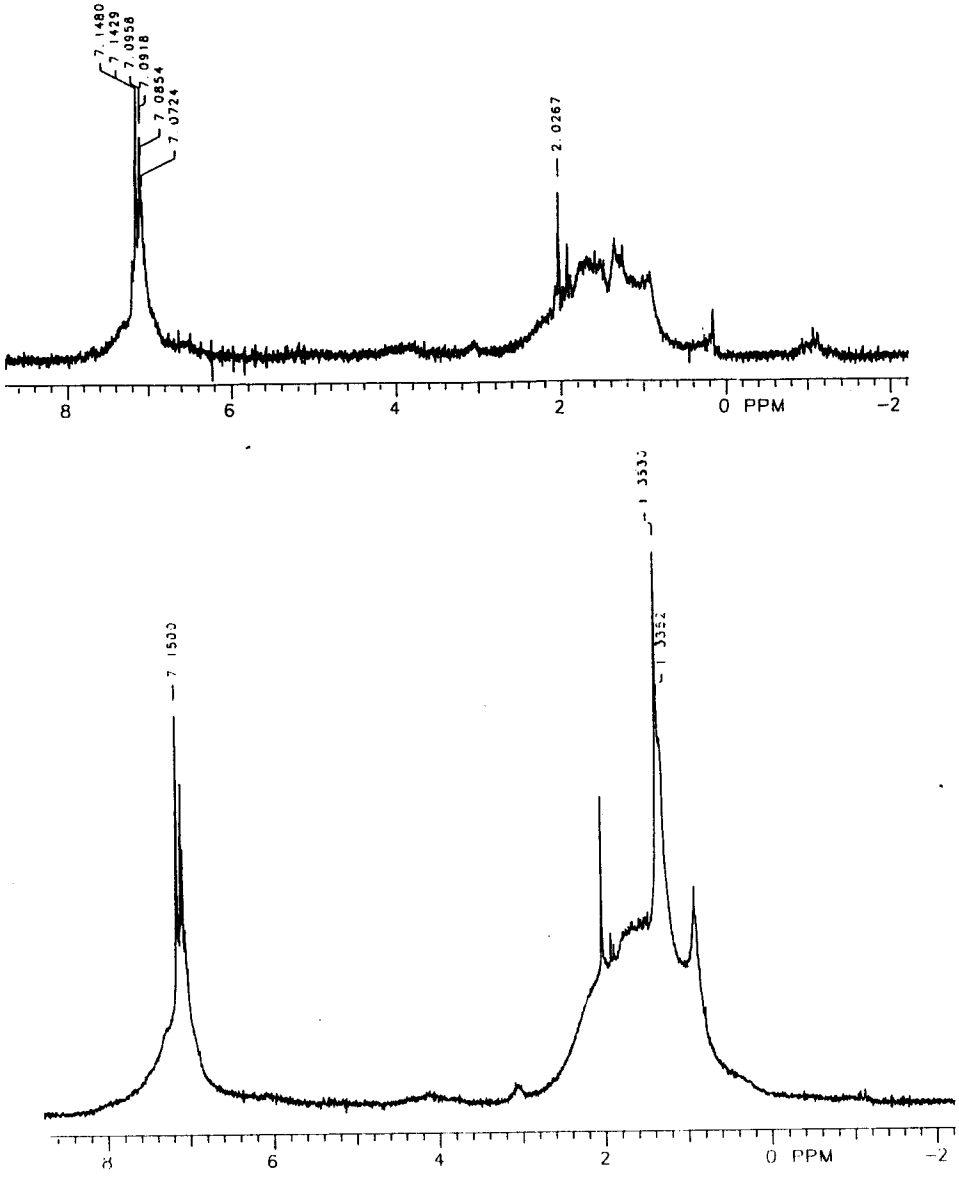

Figure 5. ^{1}H-NMR of a reaction mixture of **6/7** with **9**: (a) 30 min after mixing, (b) with the addition of propylene.

duce the cationic intermediate *anti*-[ethylidene(1-η^5-tetramethylcyclopentadienyl)(1-η^5-in-denyl)]-methyltitanium(IV) tetrakis(pentafluorophenyl)-borate (**10**).[22] Immediately upon the mixing of the reactants, there was a decrease of the Ti—Me(1) resonance as compared to that of the Ti—Me(2). At the same time a singlet at 2.0 ppm and a multiplet at around 7.1 ppm appeared due to the methyl and phenyl protons of 1,1,1-triphenylethane, respectively. After 30 min the spectrum [Fig. 5(a)] showed the two Ti—Me resonances to have very low intensities and they were broad. The aliphatic proton region was also significantly broadened. Addition of propylene gave Figure 5(b) which exhibited the new sharp resonances of PP. As in the case of reactions involving **6** and MAO (*vide supra*), no resonances were seen in spectral region expected for **10**.

Polymerizations

Numerous propylene polymerizations were performed at temperatures (T_p) of −20, 0, and 25°C for [**6**] = 27 μM and [MAO] = 54 mM ([Al]/[Ti] = 2000) in 100 mL toluene. The results are summarized in Tables III–V.

The increase of yield (Y) with time (t_p) is illustrated in Figure 6. The data afforded a calculation of variation of R_p (rate of polymerization) with t_p. Figure 7 showed that R_p actually increases with a decrease of temperature.

The concentration of propagating species, [C*], has been determined by radiolabeling with tritiated methanol for a variety of heterogeneous[23,24] and homogeneous[25] ZN-catalysts. The kinetic isotope effect is assumed to be 1.53 found for the **4**/MAO catalyst system.[8b] The variations of metal polymer bond concentration ([MPB] = [Zr—P] + [Al—P]) with Y are plotted in Figure 8. The intercept gives [C*] values listed in Table VI expressed both in concentration and as % of Ti (**6**). The amount of C* decreases with decreasing T_p. The values of k_p were calculated from the maximum $R_{p,m}$ by $k_p = R_{p,m}/[C^*][M]$ where [M] is the pro-

Table III. Propylene Polymerization at 25°C

Time (min)	Δt (min)	Y (g)	ΔY (g)	$\Delta Y/\Delta t$ (g/min)	$R_p \times 10^5$ (M/s)
0.5	0.5	0.02	0.02	0.04	15.3
1	0.5	0.05	0.03	0.06	23.8
2	1	0.08	0.03	0.03	11.9
3	1	0.1	0.02	0.02	7.93
4	1	0.12	0.02	0.02	7.93
5	1	0.14	0.02	0.02	7.93
6	1	0.15	0.01	0.01	3.96
2	1	0.17	0.02	0.02	—
8	1	0.18	0.01	0.01	3.96
9	1	0.19	0.01	0.01	3.96
10	1	0.20	0.01	0.01	3.96
20	10	0.27	0.07	0.007	2.77
30	10	0.30	0.03	0.003	1.19
40	10	0.32	0.02	0.002	0.79
50	10	0.33	0.01	0.001	0.39
60	10	0.34	0.01	0.001	0.39

Table IV. Propylene Polymerization at 0°C

Time (min)	Δt (min)	Y (g)	ΔY (g)	$\Delta Y/\Delta t$ (g/min)	$R_p \times 10^5$ (M/s)
0.5	0.5	0.04	0.04	0.08	31.7
1	0.5	0.1	0.06	0.12	47.6
2	1	0.20	0.1	0.1	39.7
3	1	0.26	0.06	0.06	23.8
4	1	0.32	0.06	0.06	23.8
5	1	0.33	0.06	0.06	23.8
6	1	0.43	0.02	0.02	—
7	1	0.51	0.05	0.02	—
8	1	0.52	0.04	0.04	15.9
9	1	0.55	0.03	0.03	11.9
10	1	0.58	0.03	0.03	11.9
20	10	0.75	0.17	0.17	6.74
30	10	0.83	0.08	0.008	3.17
40	10	0.87	0.04	0.004	1.58
50	10	0.88	0.01	0.001	0.39
60	10	0.89	0.001	0.001	0.39

Table V. Propylene Polymerization at −20°C

Time (min)	Δt (min)	Y (g)	ΔY (g)	$\Delta Y/\Delta t$ (g/min)	$R_p \times 10^5$ (M/s)
0.5	0.5	0.1	0.1	0.20	79.4
1	0.5	0.25	0.15	0.35	139
2	1	0.45	0.20	0.20	79.4
3	1	0.54	0.09	0.09	35.7
4	1	0.60	0.06	0.06	23.8
5	1	0.63	0.03	0.03	11.9
6	1	0.66	0.03	0.03	11.9
7	1	0.69	0.03	0.03	11.9
8	1	0.71	0.02	0.02	7.93
9	1	0.74	0.03	0.03	11.9
10	1	0.76	0.02	0.02	7.93
20	10	0.89	0.13	0.013	5.15
30	10	0.96	0.07	0.007	2.77
40	10	1	0.04	0.004	1.58
50	10	1.01	0.02	0.002	0.79
60	10	1.02	0.02	0.002	0.79

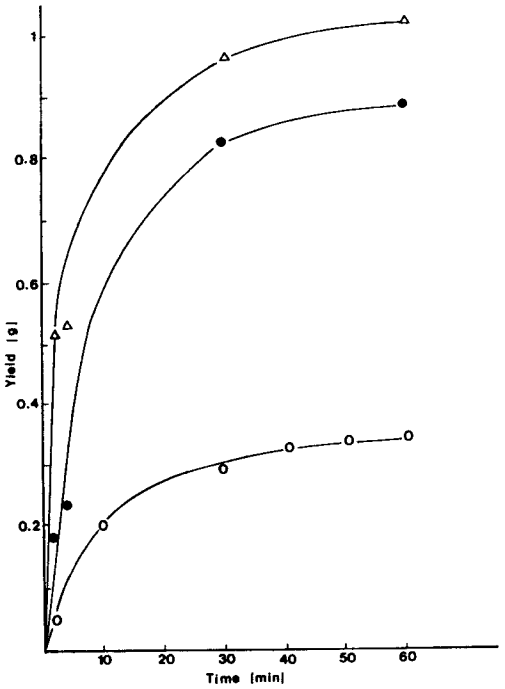

Figure 6. Variation of PP yield with time of polymerization catalyzed by **6**/MAO at: (○) 25°C, (●) 0°C, (△) −20°C.

pylene concentration which had been previously determined as a function of temperature.[6b] The slopes in Figure 8 correspond to $k_{tr}^{A}/(k_p[M])$; the results are also given in Table VI.

The MW of PP increased with t_p for low T_p of 0 and −20°C. However, it is nearly constant throughout a batch polymerization at +25°C (Fig. 9 and Table VII). PP(25) and PP(0) are insoluble in refluxing acetone but completely soluble in refluxing diethyl ether. PP(−20) is less homogeneous having 62% soluble in diethyl ether and 38% soluble in refluxing *n*-pentane.

The R_p decays rapidly as shown in Figure 7. The order of the deactivation processes depends on T_p. At the higher temperatures the decays are first order processes [Fig. 10(a)]; it is second order at −20°C [Fig. 10(b)].

Rheological Properties

Rheological properties have been investigated on PP samples obtained at T_p = −20, 0, and 25°C which are designated as PP(−20), PP(0), and PP(25), respectively. The results of storage modulus (G') and the loss modulus (G'') measurements from 30 to 200°C for PP(−20) and PP(0) obey time-temperature superposition. $G'(\omega)$ and $G''(\omega)$ measured

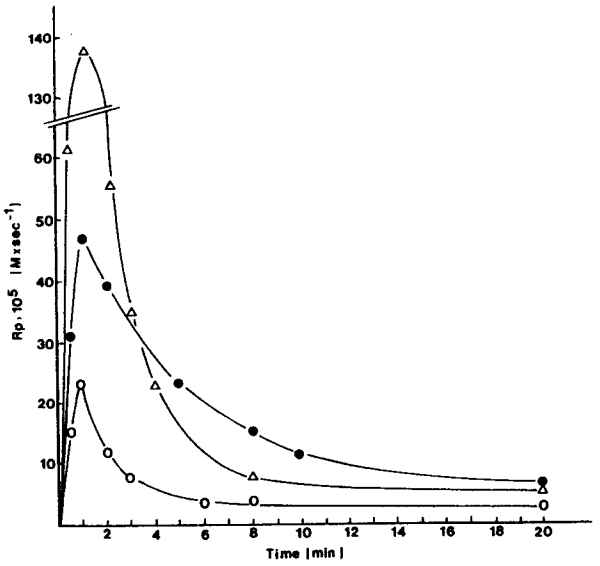

Figure 7. Variation of rate with time of polymerizations catalyzed by **6**/MAO. Symbols are the same as in Figure 6.

at different temperatures can be superposed by shifting along the frequency axis by temperature shift factor a_T, i.e., $G'(a_T\omega, T) = G'(\omega_0, T_0)$ and $G''(a_T\omega, T) = G''(\omega_0, T_0)$, where ω_0 is reduced frequency and T_0 is reference temperature. Figures 11 and 12 are the resulting master curves for the PP(−20) and PP(0) materials, respectively. These results imply that these materials do not undergo a

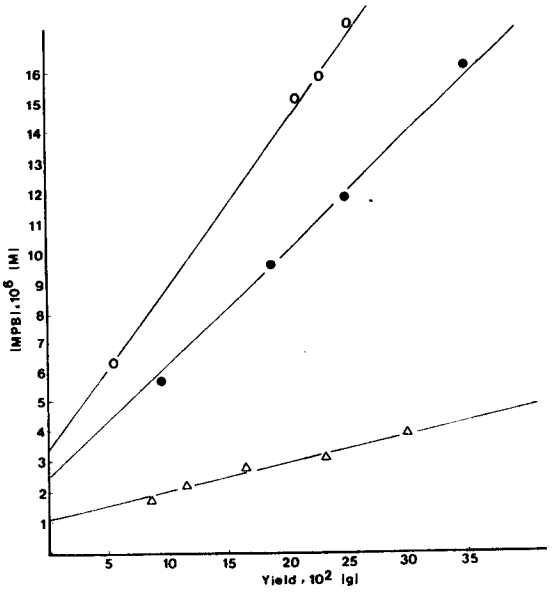

Figure 8. Variation of [MPB] vs. Y; symbols are the same as in Figure 6.

Table VI. Kinetic Results of Propylene Polymerization

	Catalyst System					
	4/MAO			6/MAO		
T_p (°C)	25	0	−20	25	0	−20
$R_p \times 10^4$ (M s^{-1})	1.2	2.0	3.4	2.4	4.8	13.9
[C_3H_6] (M)	0.47	0.73	0.94	0.47	0.73	0.94
[C*] $\times 10^6$ (M)	1.2	1.15	1.0	3.3	2.4	1.0
[C*] (% of Ti)	4.5	4.25	3.8	12.2	8.8	3.8
k_p (M s)$^{-1}$	211	236	362	153	272	1477
$k_{tr}^A \times 10^2$ (s)$^{-1}$	1.5	0.9	0.40	0.38	0.79	1.52
$k_d^a \times 10^3$ (s)$^{-1}$	5.7	4.4	3.8	3.35	2.6	
k_d^b (M s)$^{-1}$						29.6

[a] First-order rate constant
[b] Second-order rate constant.

phase transition indicating very low fractions of crystallizable sequences in the two polymers. In contradistinction, PP(25) contains a significant fraction of crystallizable sequences. A temperature sweep shows a melting transition at 63°C (Fig. 13). However, the master curve of even fully crystallized PP(25) does not exhibit a low frequency plateau for G' (Fig. 14). This indicates that the crystal domains act only as weak crosslinks in this polymer. In a supercooled state cooled from 100°C, dynamic data measured below T_m follows time–temperature superposition (Fig. 15). The temperature shifting factors for PP(−20), PP(0), and supercooled PP(25) are very close to each other over a wide temperature range (Fig. 16). For PP(25), the crystallized state has a larger a_T value than the supercooled state (Fig. 17).

The storage modulus approaches a plateau value (G_N°) for large $a_T\omega$ (Fig. 18). This is due to entanglements between molecular chains (M_e). According to the rubber elasticity theory, G_N° is related to M_e by

$$M_e = \rho RT/G_N^0 \qquad (1)$$

For $G_N^\circ = 6.5 \times 10^5$ Pa, ρ (density) $= 9 \times 10^5$ g m^{-3}, R (gas constant) $= 8.3$ N m^3 K^{-1}, $T = 303$ K, the value of M_e is 3000 g mol^{-1}.

Near the dynamics induced glassy zone, the $G''(\omega)$ for chains with a characteristic molecular weight, $M_c \approx 2\,M_e$, can be approximately described by sim-

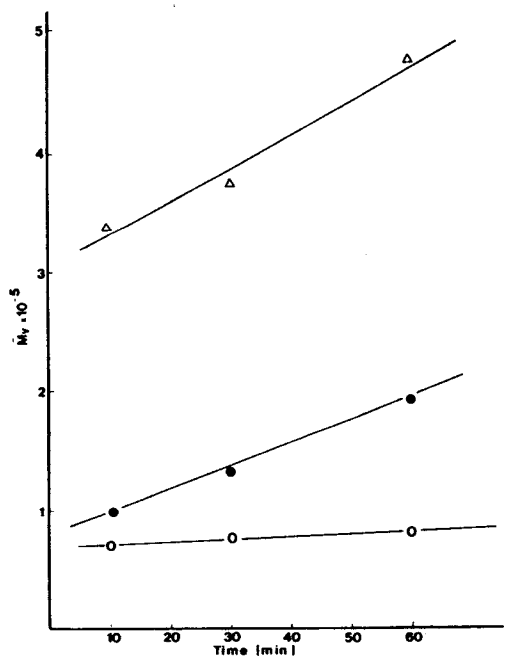

Figure 9. Variation of polypropylene molecular weight versus time of polymerization; symbols are the same as in Figure 6.

Table VII. Molecular Weight of Poly(propylene)s

T_p (°C)	t_p (min)	[η] (g dL^{-1})	$\bar{M}_v \times 10^{-4}$
−20	10	2.65	33.8
	60	3.48	47.5
0	10	1.00	10.0
	60	1.70	19.4
25	10	0.72	6.6
	60	0.80	7.6

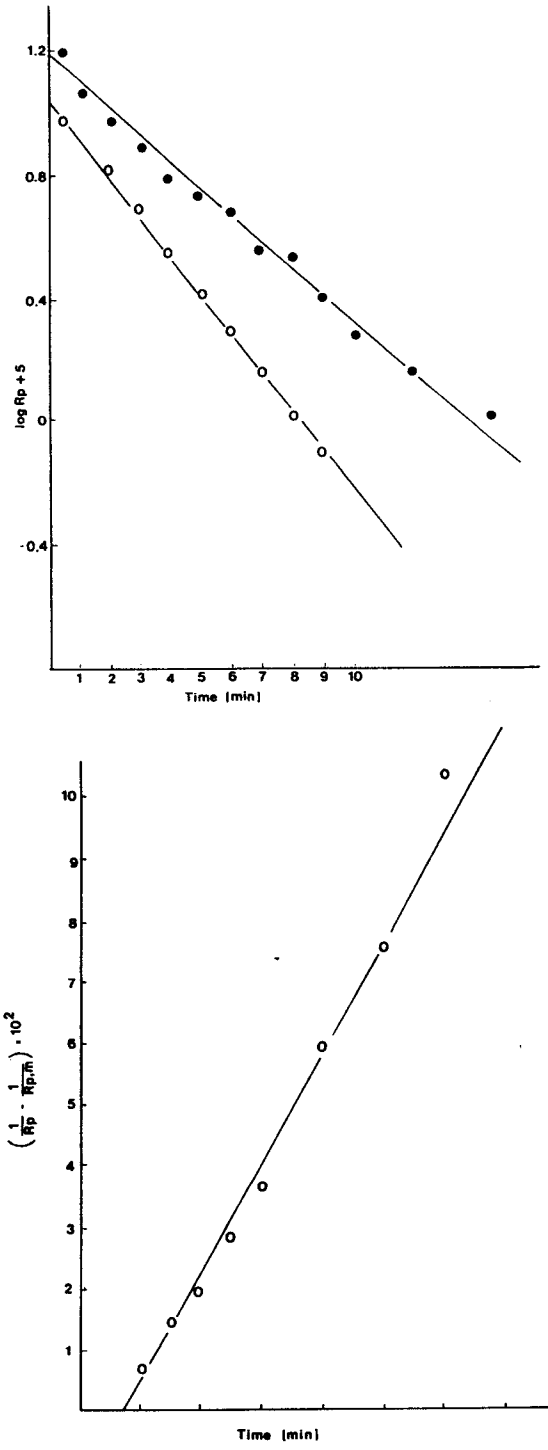

Figure 10. Decay of R_p vs. t_p: (a) first-order kinetic plot for data at (○) 20°C, (●) 0°C; and (b) second-order kinetic plot for data at −20°C.

ply shifting the flow regime G'' master curve to connect with the glassy zone G'' master curve as shown in Figure 19. It was reported[26] that above M_c the longest relaxation time τ_{max} is proportional to $M^{3.5}$.

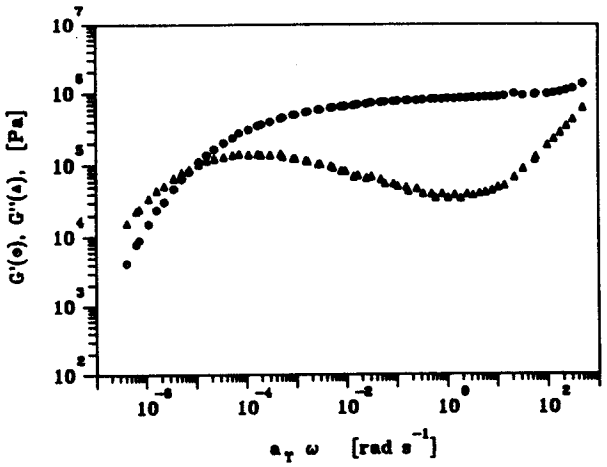

Figure 11. G' and G'' master curves of PP(−20); T_{ref} = 30°C.

From the G'' master curves, log $(\tau_{max}/\tau_{max,c})$ can be determined by log (ω_c/ω), where ω_c and ω are the frequencies at which the chains with M_c and unknown M_w have the same flow region G'' value,

$$\log(M_w/M_c)^{3.5} = \log(\tau_{max}/\tau_{max,c}) = \log(\omega_c/\omega) \quad (2)$$

From Figure 19, the values of log (ω_c/ω) are found to be 6.47, 5.16, and 3.16 for PP(−20), PP(0), and PP(25), respectively. Since $M_c \approx 2M_e \approx 6000$ g mol^{-1}, the molecular weights of the three polymers are estimated to be 4.2×10^5, 1.8×10^5, and 4.8×10^4 for PP(−20), PP(0), and PP(25), respectively, which are in good agreement with the $\bar{M}_v$ values 3.8×10^5, 1.3×10^5, and 7.5×10^4 obtained from intrinsic viscosity.

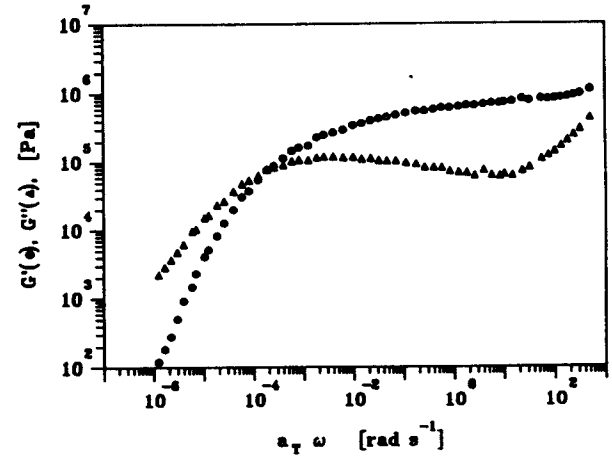

Figure 12. G' and G'' master curves of PP(0); T_{ref} = 30°C.

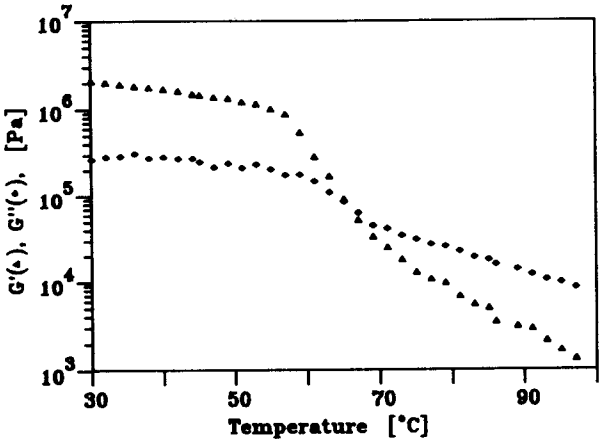

Figure 13. G' and G'' for PP(25) measured at 1 rad/s and strains within the linear viscoelastic region and a heating rate of 1 K/min.

DISCUSSION OF RESULTS

Breslow and Newburg[27a] discovered the first homogeneous ZN-catalyst: Cp_2TiCl_2/R_2AlCl. Both the neutral electron-deficient bridged complex and the ion-couple were proposed to be the active species.[27] The existence of the latter was demonstrated by electrodialysis polymerization experiments.[28] Many cationic metallocene derivatives of group 4 elements have been recently synthesized[29] and their crystal structure determined.[30] These compounds exhibit poor to modest ethylene polymerization activities but none was reported to be able to polymerize propylene stereoselectively.

Using a procedure rigorously excluding catalyst poisons and very low T_p, we were able to generate *in-situ* a "cationic" metallocene alkyl (**11**) by the following reaction:[14,22]

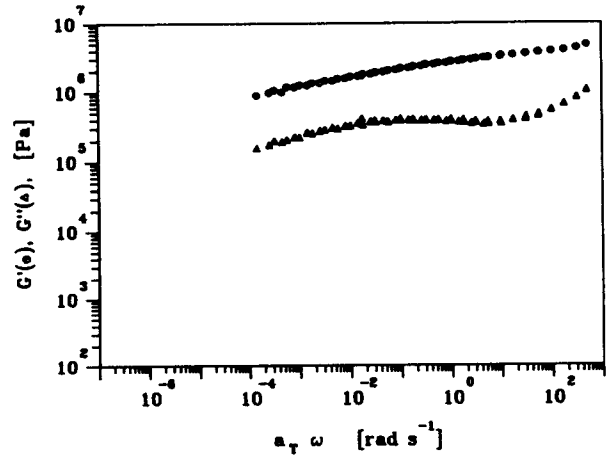

Figure 14. G' and G'' master curves of fully crystallized PP(25); T_{ref} = 30°C.

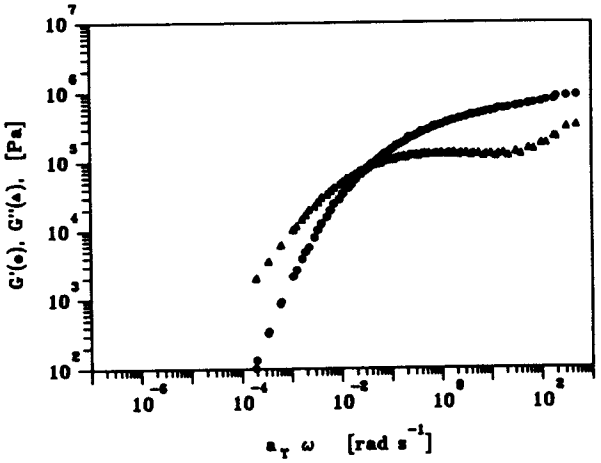

Figure 15. G' and G'' master curves of PP(25) melt or supercooled melt; T_{ref} = 30°C.

$$\text{Et[Ind]}_2\text{ZrMe}_2\textbf{(10)} + \text{Ph}_3\text{C}^+\text{B}(\text{C}_6\text{F}_5)_4^-\textbf{(9)} \rightarrow [\text{Et[Ind]}_2\text{ZrMe}]^+[\text{B}(\text{C}_6\text{F}_5)_4]^-\textbf{(11)} + \text{Ph}_3\text{CM}_e \quad (3)$$

This catalyst system is extremely active and stereoselective for propylene polymerization at −55°C. Near room temperature this "cationic" system and the **1**/MAO system polymerize propylene with comparable stereospecificity and activity. It is likely that "cationic" species may also be produced by the reaction between **1** and MAO,

$$\text{Et[Ind]}_2\text{ZrCl}_2\textbf{(1)} + \text{MAO} \rightarrow [\text{Et[Ind]}_2\text{ZrMe}]^+[\text{MAO}\cdot\text{Cl}]^- \quad (4)$$

Consequently it may be postulated that the reaction between **6** and MAO in this paper and the reaction between **4** and MAO[8] produce the same "cationic" species **12** shown in Scheme 1.

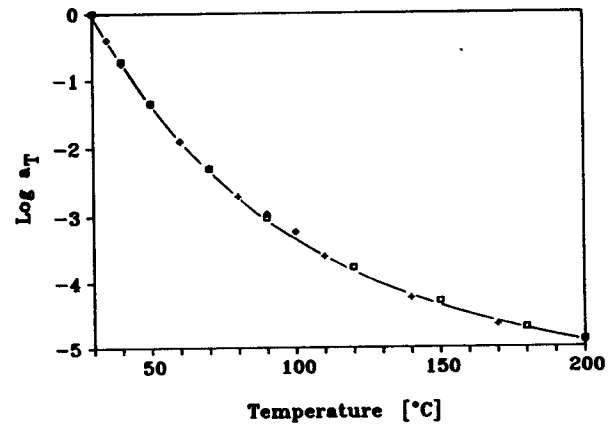

Figure 16. Temperature shifting factors of: (□) PP(−20), (+) PP(0), and (◇) supercooled liquid PP(25); T_{ref} = 30°C.

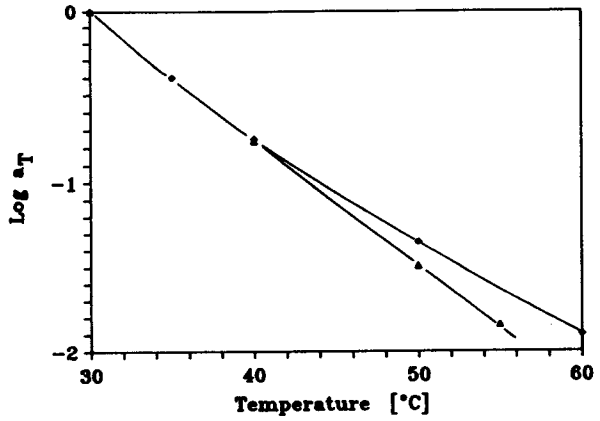

Figure 17. Comparison of temperature shifting factor of PP(25): (◇) fully crystallized, (△) supercooled liquid.

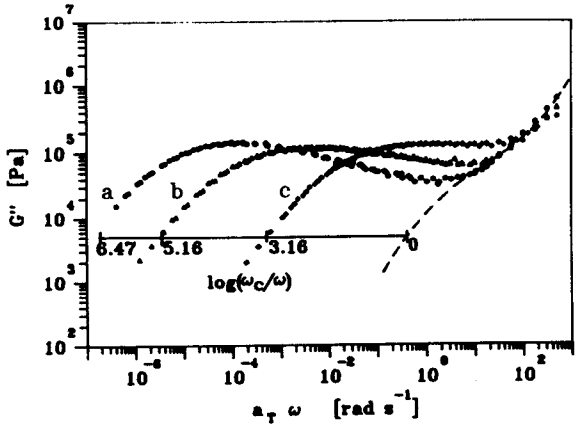

Figure 19. G'' master curves of: (a) PP(−20), (b) PP(0), and (c) supercooled PP(25). The dashed line represents $G''(\omega)$ of PP of M_e.

The formation of **12** from **4** and MAO follows simply the alkylation of Zr and elimination of chloride ion by MAO. The results of Table VI showed the production of **12** by **6** and MAO is equal to (at −20°C) or greater than the efficiencies of its formation from **4** and MAO at $T_p \geq 0$°C. The mechanism of the reaction is unknown.

The trend of increase of catalytic activity with the decrease of T_p is unprecedented in Ziegler–Natta catalysis which always show the opposite kinetic dependence until this work. More thorough studies have been made on *rac*-$C_2H_4[Ind]_2Zr^+R$[14] and *rac*-$Me_2Si[Ind]_2Zr^+R$.[31] They both show propylene polymerization activity which decrease with the increase of $T_p > -20$°C and the opposite relationship for $T_p < -20$°C. These behavior may be explained by a reversible olefin π-complexation preceeding the cis migratory insertion. This is analogous to the simplest enzyme reaction mechanism of single-substrate-to-single-product which also has similar rate-temperature variations. We must point out that some olefins were polymerized with almost no rate-T_p dependence and others with positive relationship.[31] The variation is probably due to the stability of the metallocene olefin complex.

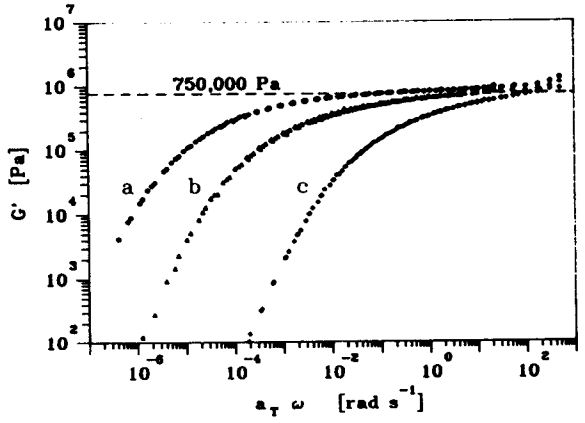

Figure 18. G' master curves of: (a) PP(−20), (b) PP(0), (c) supercooled PP(25). The dashed line represents the value of elastic plateau of entanglement coupling.

The PP produced by **6**/MAO at 25°C, PP(25), exhibits excellent elastic properties: strength = 68 MPa at elongation to break = 850%, stress at 100% elongation = 3.0 MPa, and recovery after 100% elongation = 95%. However, it has a lower content of crystallizable stereoregular sequence than the PP′(25) produced by **4**/MAO. Prime is used to denote polymer produced by **4**/MAO and its properties; it is omitted for **6**/MAO cases. The former has a T_m (melting temperature) for the *cry* (crystalline) domains of 62°C as compared to T'_m = 65°C for the latter. Another difference is the absence of an equilibrium modulus for PP(25) while the PP′(25) has a value of 0.56 MPa for the equilibrium modulus. These properties suggest that the average length of the crystallizable segments in the PP(25) to be shorter than those in the PP′(25). This difference extends to the PP produced at 0°C by the two catalysts. Time–temperature superposition between 50 and 120°C was not applicable to PP′(0) obtained

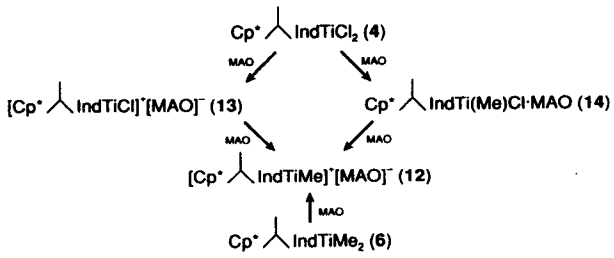

Scheme 1. Formation of "cationic" catalytic species **12** from **4**/MAO or **6**/MAO.

with **4**/MAO indicating it to contain certain amount of crystallizable sequences which melt in the said temperature range. For PP(0) produced by **6**/MAO, time–temperature shifting applies to all temperatures > 25°C. There is no significant melting transition in this material. The steric microstructures of the thermoplastic elastomeric polymer (TPE–PP) is a sensitive measure of the propagation behaviors of the catalyst producing it. The important point is that **6**/MAO also produces stereoblock PP having alternating crystallizable/stereoregular and amorphous/stereoirregular sequences like the PP′ obtained with **4**/MAO. This type of polymer microstructure cannot be produced by a "single-site" catalyst with only one stereochemical mode for regulation of monomer insertion. One can readily envisualize the nonsymmetric *ansa*-complexes **4** or **6** to be "dual-site" catalysts.

The two Ti—Me groups are grossly different. The x-ray structure of **6** showed Me(2) to be situated directly beneath the C_6 ring of indenyl whereas Me(1) is not under the influences of any ring current field. The methyl resonances A and B in Figure 3 are assigned to Me(1) and Me(2), respectively, in the anti-diastereomer. The resonances A′ and B′ in Figure 3(a) are due the corresponding methyls in the *syn* compound **7**. The ethylidene methyl C′ in this compound is appreciably shifted downfield compared to the corresponding methyl C for **6** in Figure 3(b) probably because of a ring-current field effect on this methyl group in the *syn* derivative.

The addition of **9** to the diastereomeric mixture of **6** and **7** in a NMR sample tube caused the appearance of red oily droplets. Even though the proton resonances (methyl at 2.0 ppm and phenyl at 7.1 ppm) of the expected product $(Ph)_3CCH_3$ were observed, no signal attributable to a Ti—Me^+ resonance could be found. The spectra of the reaction mixture of **6** and **7** with MAO shows a proton resonance of MAO which shifts to lower field with time of reaction. This shift is consistent with the electron deficient bonding with the chloride ion. In both these reactions the Ti—Me(1) resonance is affected more than Ti—Me(2).

We postulate that the catalytic species exists in two isomeric states:

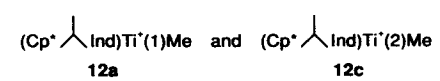

12a **12c**

where the Ti(1)Me and Ti(2)Me become Ti(1)P and Ti(2)P during propagation. Based on the x-ray structure, these is less nonbonded interaction for Ti(1)P than Ti(2)P and the propagation is less stereoselective in the former than the latter. Ti(1)P and Ti(2)P produce amorphous/stereoirregular and crystallizable/stereoregular PP segments, respectively:

$$\mathbf{12a} + a C_3H_6 \xrightarrow{k_{p,a}} \mathbf{12a}(am\text{-PP})_a\text{Me} \qquad (5)$$

$$\mathbf{12c} + c C_3H_6 \xrightarrow{k_{p,c}} \mathbf{12c}(cry\text{-PP})_c\text{Me} \qquad (6)$$

The isomerization (site-switching) occurs several times during the growth of the PP chain.

$$\mathbf{12a} \underset{k_{-1}(C_3H_6)}{\overset{k_1(C_3H_6)}{\rightleftarrows}} \mathbf{12c} \qquad (7)$$

If the isomerization is accompanied by a monomer insertion, then the stereoblock lengths are simply $a = k_{p,a}/k_1$ and $c = k_{p,c}/k_{-1}$. Otherwise the ratio of rate constants is multiplied by $[C_3H_6]$.

The mechanical properties are governed by the microstructures which are produced according to reactions (5)–(7). Stereoblock PP is produced at 25°C which possesses excellent mechanical and elastic properties. Physico-mechanical[8] and ^{13}C-NMR[32] found it to certain many alternating (30 or more) blocks of *am*-PP and *cry*-PP of sufficient lengths, 50 and 20 monomer units, respectively. At T_p 50°C, the TPE–PP obtained has twice the block lengths of the former but only one-third as many blocks with consequent lower mechanical properties.[8] According to reactions (5)–(7) the ratio of $k_p[M]/k_i (i = 1, -1)$ is greater at higher T_p. Conversely, the ratio is smaller at low T_p leading to very large number of short blocks. In particular the stereoregular blocks become too short to crystallize; the materials is without TPE characteristics.

This work was supported by the Materials Research Laboratory at the University of Massachusetts, Amherst.

REFERENCES AND NOTES

1. (a) Part I: J. C. W. Chien and B. P. Wang, *J. Polym. Sci. Part A: Polym. Chem.*, **26**, 3089 (1988); (b) Part XXII: J. C. W. Chien, W.-M. Tsai, and M. D. Rausch, *J. Am. Chem. Soc.*, **113**, 8570 (1991).
2. (a) J. C. W. Chien, *J. Polym. Sci. A-1*, **1**, 425, 1839 (1963); (b) G. Natta, *J. Polym. Sci.*, **34**, 21 (1959).
3. (a) J. C. W. Chien, J. C. Wu, and C. I. Kuo, *J. Polym. Sci. Polym. Chem. Ed.*, **20**, 2019 (1982) described the third generation Ziegler–Natta catalyst; (b) Y. Hu and J. C. W. Chien, *J. Polym. Sci. Part A: Polym. Chem.*, **26**, 2003 (1988) introduced the fourth generation Ziegler–Natta catalyst.
4. (a) W. Kaminsky, K. Külper, H. H. Brintzinger, and F. R. W. P. Wild, *Angew. Chem. Int. Ed. Engl.*, **24**, 507 (1985); (b) W. Kaminsky, *Angew. Makromol. Chem.*, **145/146**, 149 (1985); W. Kaminsky, in *Catalytic Polymerization of Olefins*, T. Keii and K. Soga, Eds. Kodansha Elsevier, Tokyo, 1986, p. 293.